Proceedings of 10th International Conference on Precision, Meso, Micro and Nano Engineering (COPEN 10)
December 07 – 09, 2017, Indian Institute of Technology Madras, Chennai – 600 036 INDIA

Microstructural characterization and its effect on mechanical properties of fiber laser beam welded Ti-6Al-4V alloy

Chandan Kumar, Manas Das*

Department of Mechanical Engineering
Indian Institute of Technology, Guwahati - 781039, Assam, INDIA

Abstract

Titanium and its alloys serve as a bridge between the ideal properties of aluminium and steel. It possesses unique characteristics such as, higher specific strength, better corrosion resistance, and excellent biocompatibility. Therefore, it is widely used in aviation, aerospace, chemical and medical industries, etc. In this paper, experimental investigations of fiber laser beam welded specimens of Ti-6Al-4V alloy are carried out. After experiments, the depth of penetration, microstructure and the mechanical properties of the laser welded specimens are investigated. The microstructure of the fusion and heat affected zone changes after laser beam welding which are strongly influenced by the welding power. The mechanical properties of the welded specimens are greatly dependent on the developed microstructure in the fusion and heat affected zones. A logical approach is developed to correlate the variation in mechanical properties like hardness and tensile strength with microstructural variation at different regions of the welded joint. The results show that welding power plays the major role for full penetration i.e. keyhole mode of welding which produces full penetration, narrower weld width, small HAZ and good weld appearance with acceptable mechanical properties.

Keywords: Laser beam welding, Ti-6Al-4V alloy, Microstructure, Hardness, Tensile strength

1. INTRODUCTION

Titanium is the 4th most abundant structural material on the earth planet. It exists in two crystal forms i.e. α phase having hexagonal close packed (HCP) structure and β phase having body centered cubic structure (BCC). The allotropic transformation takes place in unalloyed titanium at above 882°C known as transition temperature. Titanium alloys are divided into four categories i.e. α alloy, near α alloy, α+β alloy and β. Ti-6Al-4V (Ti64) alloy falls in the category of two phase alloy i.e. α+β phase. It has good combination of strength and ductility. It is extensively used in many areas such as, aerospace, medical, chemical and aviation industries because of its high specific strength, low density, good elevated temperature properties, better corrosion resistance and excellent biocompatibility. The thermal conductivity of Ti64 is very poor. However, its heat of fusion and the heat of vaporization are higher than iron. Due to lower thermal conductivity and higher heat of fusion and heat of vaporization, welding of Ti64 alloy using conventional fusion welding techniques is very difficult because of its higher tendency to react with atmospheric gases such as H_2, O_2 and N_2 at higher temperature which enhances welding defects [1, 2].

Welding is the utmost flexible joining technology which is applicable for the fabrication of several products used in many industries. Different types of energy sources are used for welding such as gas flame, electric arc, laser beam, electron beam and ultrasound. Laser beam welding (LBW) is one of the most important type of non-conventional and advanced joining methods for joining similar or dissimilar materials. It is a promising joining technology having high beam quality, high precision, high performance, high speed, good flexibility and low deformation. Different types of laser heat sources are available for welding purposes i.e. CO_2, Nd: YAG, diode and recently developed fiber laser. Fiber laser beam welding is a high energy density and very low heat input process. It is a promising alternative to the conventional solid state laser system. The fiber laser offers several advantages compared to other lasers as high efficiency, high beam quality, long life, compact size and lower operating cost [2-3].

Several researchers did microstructural characterization of laser beam welded Ti64 alloy. Akman et al. did microstructural study of Nd-YAG laser beam welded Ti64 alloy [4]. They reported that acicular martensite (α′) in the fusion zone (FZ) and the mixture of α′ martensite, acicular α and primary β is formed in the heat affected zone (HAZ). Caiazzo et al. investigated the laser beam welded butt joint of Ti64 alloy. They reported that the microstructure of fusion zone consists of acicular α′ martensite. They reported that fusion zone area is not affected by the defocusing distance, although bead profile does [5]. Pan et al. reported that similar or slightly higher joint strength is achieved in LBW as compared to base metal (BM) at the expense of ductility. The decrease in ductility is due to the presence of micro pores and aluminum oxide inclusions [6]. There are huge numbers of parameters involved in fiber LBW process which affect weld quality as shown in Fig. 1. The most vital process parameters are LBW power, welding speed, defocused position and flow rate of shielding gas.

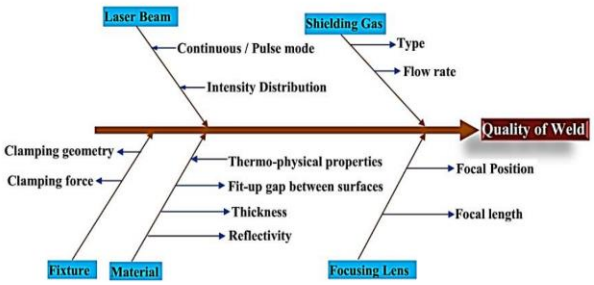

Fig. 1. LBW process parameters

*Manas Das, Email: manasdas@iitg.ernet.in

ISBN: 978-93-80689-28-9

2. EXPERIMENTAL ANALYSIS

In the present study, an experimental investigation of fiber LBW of Ti-6Al-4V (Ti64) alloy is carried out at different welding power to understand its effect on mechanical and metallographic properties of the joint. The chemical composition of Ti64 alloy is listed in Table 1. The schematic diagram of workpiece dimension and LBW experimental setup are shown in Figs. 2 (a) and (b), respectively.

Before welding, the workpiece surfaces are chemically cleaned using acetone to eliminate contamination with dirt and grease. The edges of the workpieces are milled using milling machine to reduce the fit up gap between two workpieces. Afterward, the workpieces are mounted on a clamping device to reduce distortion and displacement during welding. The fiber LBW experimental conditions and machine configurations are listed in Table 2.

Table 1: Chemical composition of Ti64 base metal

Element	Al	V	C	Si	O	Ti
Wt.%	5.8	3.8	0.08	0.2	0.21	Balance

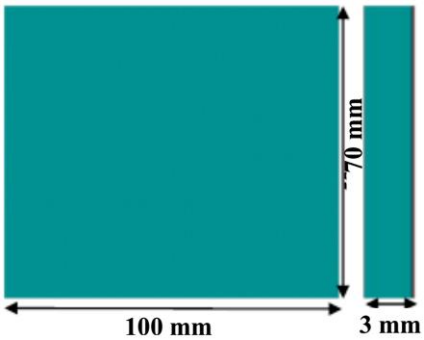

(a)

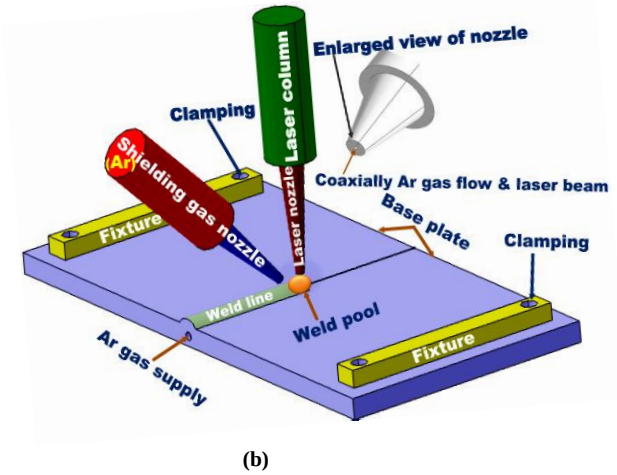

(b)

Fig. 2. Schematic of (a) workpiece dimension and (b) LBW setup

Argon gas is used as a shielding gas to suppress the plasma and to protect the weld pool and heated surface from the detrimental impact of atmospheric air and environmental contamination such as oxidation. The fixed and variable parameters are given in Table 3.

Preliminary experiments are conducted to perform the feasibility study of the fiber LBW of Ti64 alloy plates. From the literature, it has been found that Ti64 is highly oxidized while welding under atmospheric condition. Hence, special care has to be taken to protect the weld pool to inhibit oxidization during and after welding. Experiments are carried out at three different welding power at 500 mm/min constant welding speed under shielding gas environment (i.e. Ar) as listed in Table 3.

Table 2: Fiber LBW machine configurations

Mode of laser power	Continuous wave
Beam mode	Multi- mode
Spot diameter	200 µm on top surface
Wavelength	1080 nm
Beam incident angle	90º
Type of shielding gas	Argon
Flow rate of Argon	10 LPM
Fiber core diameter	50 µm
Position of focal point	On the top surface

Table 3: Experimental conditions of LBW process

LBW power (Watt)	Exp. 1	1500
	Exp. 2	1600
	Exp. 3	1700
Welding speed	500 mm/min	

For metallographic inspection, welded specimens are cut by wire electro discharge machine (W-EDM) and it is mounted using epoxy resin and then polished on an emery paper and velvet cloth, successively. After polishing, the samples are etched with aqueous solution of Kroll's reagent (i.e. 92% distilled water, 6% HNO_3, 2% HF) by dipping it for 20 seconds at room temperature. After etching, the cross sections of the welded samples are examined for microstructural and morphological studies under optical microscope and field emission scanning electron microscope (FESEM). The Vickers micro hardness of the weld bead cross section is measured using Vickers micro hardness tester at a 200 gm constant load and 15s dwell time. Each hardness value is calculated from the average of three indentations. The tensile tests of the samples are carried out using Instron model machine with a maximum load of 10 kN at a constant strain rate of 0.5 mm/min. Also, the microstructural analysis in the welded region of the specimen is carried out.

3. RESULTS AND DISCUSSION

The experimental results at different welding conditions are discussed in the following subsections.

3.1. Effect of LBW Power

Figure 3 shows the weld bead macrographs at different welding conditions. It is observed from Fig. 3 that the depth of penetration increases with increasing laser beam welding power from 1500 to 1700 W. Full penetration in the base plate is obtained at LBW power of 1700 W (Fig. 3(c)). The weld beads show the characteristics of keyhole mode of welding process. No bulks cracks are found in the weld bead anyone of the samples. It may be partly due to the excellent crack resistance of the base metal and the LBW conditions at which experiments are carried out. It is also observed from the macrographs of welded specimens (Fig. 3) that the weld pool is symmetrical about the axis of the laser beam. The lack of symmetricity is observed only in the root side of the specimens. Two opposite forces namely electromagnetic and surface tension forces act in the weld pool. At this location, electromagnetic force may

overcome surface tension force influencing convective heat transfer. As a result, any local agitation in the weld pool causes the flow field to change dramatically which may lead to unsymmetrical weld bead at the root side.

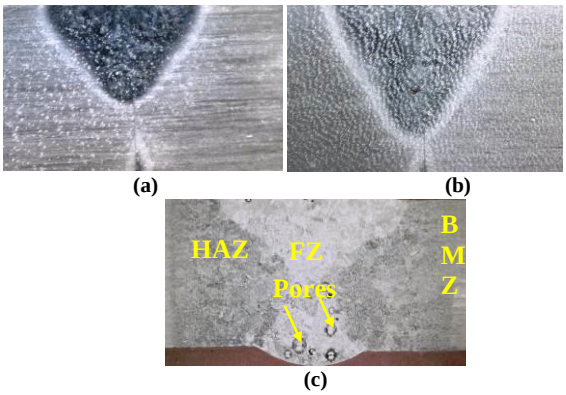

Fig. 3. Weld bead macrographs for Exp. No. (a) 1, (b) 2 and (c) 3

3.2. Microstructural Analysis

The microstructure of base metal is shown in Fig. 4. The base metal microstructure is mainly composed of two phases i.e. intergranular β phase and equiaxed α phase. The light and dark areas represent α and inter-granular β phase, respectively. The β phase is distributed along the boundaries of the HCP structure of α phase.

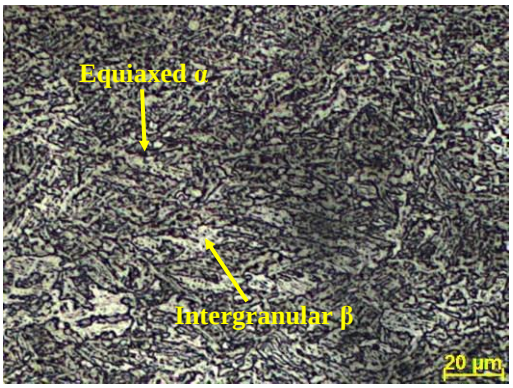

Fig. 4. Microstructure of Ti64 base metal

The optical as well as FESEM images of FZ are shown in Figs. 5 and 6, respectively for Exp. 3 (Table 3). The diffusionless transformation of β phase into α′ martensitic phase takes place in the FZ due to high cooling rate in this zone. The needle shape of the α′ lamella is shown in Fig. 6. It indicates that the cooling rate under the welding condition in Exp. 3 is above the critical limit i.e. 410°C/s for the formation of α′ martensitic phase in the FZ.

The individual points in the HAZ experiences distinct temperature gradient in terms of both maximum temperature and cooling rate during fiber LBW process. Thus, each point in the HAZ shows distinct microstructural features due to their differences in the cooling rate. Hence, non-uniform mechanical as well as metallurgical characteristics is observed in the HAZ. Figures 7 (a-d) show the FESEM images of the microstructure in the HAZ at four different locations i.e. near FZ, middle of HAZ, far away from FZ and near BMZ, respectively.

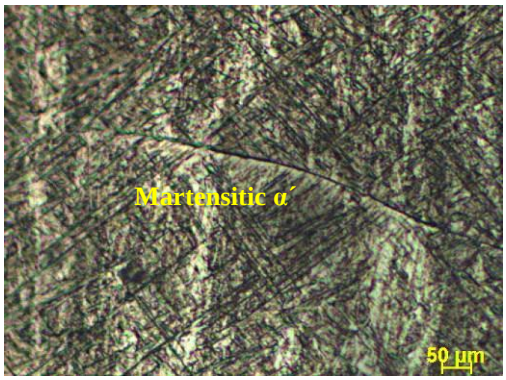

Fig. 5. Optical image of microstructure in FZ

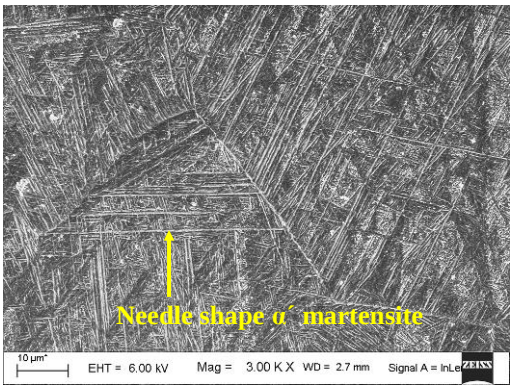

Fig. 6. FESEM image of microstructure in FZ

The near HAZ is the region where maximum temperature rises more than β transus temperature of 995°C and less than liquidus temperature of 1655°C. In this region, the mixture of acicular α′ (martensitic phase) and small amount of blocky α phases are formed and it is clearly observed in FESEM micrographs in Figs. 7(a).

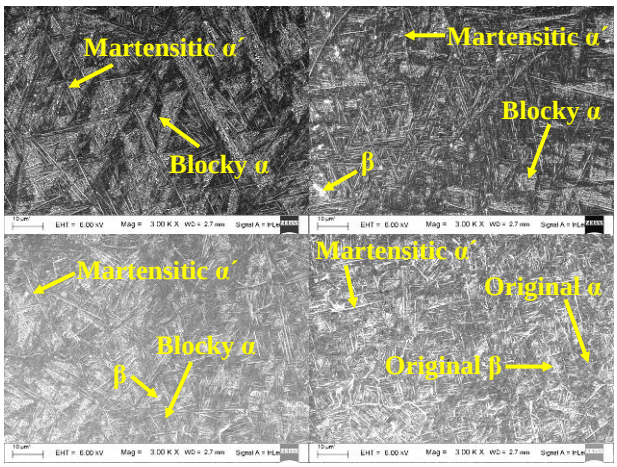

Fig. 7. FESEM images of HAZ microstructures at different locations (a) near FZ (b) middle of HAZ (c) far away from FZ and (d) near BMZ

The middle of the HAZ consists of a mixture of blocky α and primary β phases along with α′ martensitic phase as shown in Fig. 7(b). The fully transformed HAZ is not found in the middle of the HAZ due to lesser peak temperature. The HAZ which is far away from the FZ consists of a mixture of blocky α, primary

β and small amount of α′ martensitic phases as shown in Fig. 7(c). The microstructure in the HAZ near BM is fully different than near FZ and middle of HAZ as shown in Fig. 7(d). In this region, lesser amount of martensitic α′ along with original α and β phases are observed. Due to the presence of original α and β phases, this region is termed as partially transformed region. From Figs. 7(a) to (d), it is observed that the percentage of α′ phase decreases continuously from near FZ to near BMZ.

4. MECHANICAL PROPERTIES

The mechanical properties in terms of microhardness and tensile strength of the welded specimens are discussed in the present subsection.

4.1. Microhardness

Figure 8 shows the hardness distribution curve for Exp. 3 (Table 3). The micro hardness of BM is about 246 HV. Maximum hardness of the workpiece is observed at the centre of the FZ, followed by HAZ and BMZ. It is mainly due to the higher cooling rate in the FZ than the HAZ and BMZ. The higher cooling rate causes the formation of harder phase of α′martensitic structures in the FZ and HAZ.

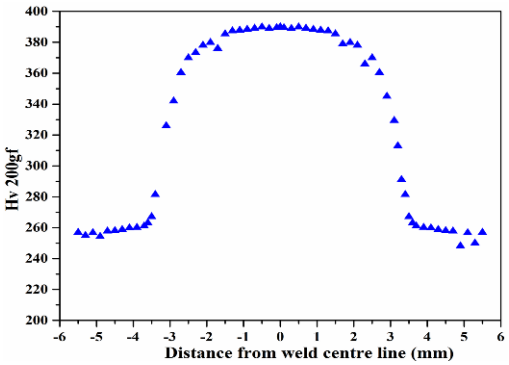

Fig. 8. Hardness distribution curve for Exp. 3 (Table 3)

4.2. Tensile Properties

The dimension of the specimen considered for tensile testing is shown in Fig. 9. The tensile testing results are given in Table 4. The tensile strength and % elongation of the welded specimen is degraded and fracture occurs in the FZ. The qualities of the welded specimens are poor due the formation of pores which acts like as a stress concentrators and leads to the initiation sites for cracks. The tensile properties of the samples can be improved by post heat treatment.

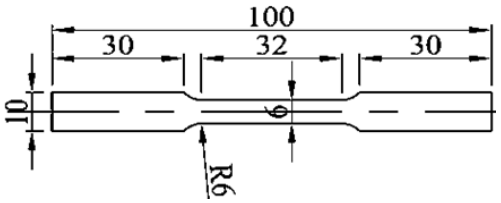

Fig. 9. (a) Schematic diagram of tensile testing specimen (All dimensions are in mm)

Table 4: Tensile testing results

	UTS* (MPa)	Young's Modulus (GPa)	% elongation
BM	980	110	11
Exp. 3	687	87.58	7.2

UTS – Ultimate tensile strength

5. CONCLUSIONS

In the present study, continuous wave fiber laser beam welding of 3 mm thick Ti-6Al-4V alloy in butt configuration is carried out at different welding power. Smooth, uniform, and shiny bead with no spatters and crack free weld is formed. The weld pool is almost symmetrical about the axis of the laser beam. The α′ martensitic microstructure is developed in the FZ. The percentage of α′ martensitic phase decreases almost 100% in the FZ to zero in the BMZ. Maximum hardness in the workpiece is observed in the FZ. The tensile strength and % elongation of the welded joint is lower than the BM of Ti64 alloy. It is mainly due to the formation of porosity in the weld bead which can be reduced by conducting welding experiments in vacuum environment. The shielding gas delivery system must be configured in such a way that both the top and back side of the welded zones are not in contact with the atmospheric gases until the surface temperature is lower than 300°C.

References

[1] J. Matthew and Jr. Donachie, A Technical Guide: 2nd Edition, Materials park, OH: ASM International, 2000.

[2] A. Costa, R. Miranda, L. Quintino, D. Yapp, Analysis of beam material interaction in welding of titanium with fiber lasers, *Materials and Manufacturing Processes*, **22** (2007) 798–803.

[3] K. Manonmani, N. Murugan, G. Buvanasekaran, Effects of Process Parameters on the Bead Geometry of Laser Beam Butt Welded Stainless Steel Sheets, *International Journal of Advanced Manufacturing Technology*, **32** (2007) 1125–1133.

[4] E. Akman, A. Demir, T. Canel, T. Sinmazcelik, Laser welding of Ti-6Al-4V titanium alloys, *Journal of Materials Processing Technology*, **21**(2009) 3705-3713.

[5] F. Caiazzo, F. Curcio, G. Daurelio, F. M. C. Minutolo, Ti-6Al-4V sheets lap and butt joints carried out by CO_2 laser mechanical and morphological characterization, *Journal of Materials Processing Technology*, **149** (2004) 546–552.

[6] L. K. Pan, C. Wang, S. L. Wei, H. F. Sher, Optimizing multiple quality characteristics via taguchi method-based grey analysis, *Journal of Material Processing Technology*, **182** (2007) 107-116.